Macedonian Journal of Chemistry and Chemical Engineering, Vol. **44**, No. 2, pp. 317–329 (2025)

MJCCA9 – 939

ISSN 1857-5552
e-ISSN 1857-5625

Received: September 16, 2025
Accepted: August 27, 2025

DOI: 10.20450/mjcce.2025.3257
Original scientific paper

ELECTROCHEMICAL AND STRUCTURAL EVALUATION OF $CoFeNiO_x$-BASED CATALYSTS FOR WATER SPLITTING APPLICATIONS

Yasir Hashmi, Jianzhi Wang, Faquan Yu

Key Laboratory for Green Chemical Process of Ministry of Education
Hubei Key Laboratory for Novel Reactor and Green Chemistry Technology
Hubei Engineering Research Center for Advanced Fine Chemicals
School of Chemical Engineering and Pharmacy
Wuhan Institute of Technology

fyu@wit.edu.cn

We report trimetallic cobalt-iron-nickel oxide ($CoFeNiO_x$) electrocatalysts prepared by a hydrothermal route followed by thermal annealing and post-synthesis alkaline activation (sodium hydroxide/potassium hydroxide/urea). By tuning the Co:Fe:Ni molar ratio (1:1:1, 1:3:1, and 3:1:1), we correlate phase composition and morphology with electrocatalytic water splitting performance. X-ray powder detraction indicates the coexistence of layered double hydroxide–derived motifs with spinel-type oxides, while scanning and transmission electron microscopy reveal increased roughness and porosity in Co-rich samples after KOH/urea treatment. In 1 M KOH, the $CoFeNiO_x$ (1:1:1) electrocatalyst exhibits the most favorable oxygen evolution reaction activity ($\eta 10$ = 264 mV; Tafel slope = 84.4 mV dec^{-1}), stable chronopotentiometry at 10 mA cm^{-2} for 24 h with a ~40 mV increase in overpotential, and low charge transfer resistance based on electrochemical impedance spectroscopy. The CoFeNiOx (3:1:1) electrocatalyst delivers the best hydrogen evolution reaction response among the tested electrocatalysts. X-ray photoelectron spectroscopy confirms mixed valence states with enrichment of trivalent species (Co^{3+}/Co^{2+}, Ni^{3+}/Ni^{2+}, Fe^{3+}/Fe^{2+}) on the surface, consistent with the formation of catalytically active oxyhydroxide layers under alkaline conditions. Overall, controlled composition coupled with urea-assisted alkaline activation enhances the exposure of active sites exposure and charge transport, enabling the production of bifunctional $CoFeNiO_x$ electrocatalysts that are suitable for integrated water-splitting systems.

Keywords: $CoFeNiO_x$, water splitting, oxygen evolution reaction (OER), hydrogen evolution reaction (HER), electrocatalysis, trimetallic oxides, Tafel slope

ЕЛЕКТРОХЕМИСКА И СТРУКТУРНА ЕВАЛУАЦИЈА НА КАТАЛИЗАТОРИ БАЗИРАНИ НА $CoFeNiO_x$ ЗА ПРИМЕНИ ВО ЦЕПЕЊЕ НА ВОДА

Во овој труд се опишани тријметални оксидни електрокатализатори на кобалт-железо-никел алкална активација (натриум-хидроксид/калиум-хидроксид/уреа). Со прилагодување на моларниот сооднос Co:Fe:Ni (1:1:1, 1:3:1 и 3:1:1), е извршена корелација на составот и морфологијата со перформансите при електрокаталитичкото цепење на водата. Рентгенската прашкаста дифракција (XRD) укажува на коегзистенција на мотиви изведени од слојни двојни хидроксиди со оксиди од типот спинел, додека скенирачката и трансмисионата електронска микроскопија (SEM и TEM) откриваат зголемена грубост и порозност во примероците богати со Co по третманот со KOH/уреа. Во 1 M KOH, електрокатализаторот $CoFeNiO_x$ (1:1:1) покажува најповолна активност за реакцијата за еволуција на кислород (OER) (η_{10} = 264 mV; Тафелов наклон = 84,4 mV dec^{-1}), стабилна хронопотенциометрија при 10 mA cm^{-2} за 24 h со зголемување на наднапонот од ~40 mV, и низок отпор при пренос на полнеж според електрохемиската импедансна спектроскопија (EIS). Електрокатализаторот $CoFeNiO_x$ (3:1:1) дава најдобар одговор за реакцијата за еволуција на

водород (HER) меѓу тестираните примероци. Рентгенската фотоелектронска спектроскопија (XPS) потврдува мешани валентни состојби со збогатување на тривалентните видови (Co^{3+}/Co^{2+}, Ni^{3+}/Ni^{2+}, Fe^{3+}/Fe^{2+}) на површината, што е во согласност со формирање на каталитички активни оксихидроксидни слоеви во алкални услови. Вкупно, контролираниот состав во комбинација со алкална активација потпомогната со уреа го зголемува изложувањето на активните места и преносот на полнеж, овозможувајќи производство на бифункционални $CoFeNiO_x$ електрокатализатори погодни за интегрирани системи за цепење на водата.

Клучни зборови: $CoFeNiO_x$, цепење на водата; реакција на издвојување на кислород (OER); реакција на издвојување на водород (HER); електрокатализа; триметални оксиди; наклон на Tafel;

1. INTRODUCTION

The global pursuit of clean and sustainable energy has intensified interest in green energy conversion technologies, particularly those that can mitigate reliance on fossil fuels and reduce greenhouse gas emissions.[1] Among these, electrochemical water splitting has emerged as a promising method for producing high-purity hydrogen and oxygen, which are key components in renewable fuel cycles and fuel cell applications. This process involves two half-reactions: the hydrogen evolution reaction (HER) at the cathode and the oxygen evolution reaction (OER) at the anode.[2] While the HER is relatively facile, the OER remains a critical bottleneck due to its sluggish kinetics, involving a complex four-electron transfer mechanism that demands high overpotentials and limits overall efficiency. To address these kinetic challenges, significant efforts have been devoted to developing efficient, cost-effective, and durable electrocatalysts.[3,4] Noble metal oxides such as iridium(IV) oxide (IrO_2) and ruthenium(IV) oxide (RuO_2) are widely considered the gold standard for OER catalysis due to their excellent activity; however, their high cost and scarcity severely hinder large-scale commercialization. Hence, researchers have turned their attention to earth-abundant transition metal oxides, including those based on cobalt (Co), iron (Fe), and nickel (Ni), which have demonstrated promising bifunctional activity for both HER and OER under alkaline conditions.

Recent studies have shown that trimetallic oxides, particularly CoFeNi-based systems, can offer enhanced electrocatalytic performance through synergistic interactions among the constituent metals.[5] For example, Zhang *et al.*[6,7] demonstrated that CoFeNi layered double hydroxides (LDH) show superior OER activity due to dynamic electron transfer between Co^{3+} and Fe^{3+} centers. Similarly, Yu *et al.*[8,9] reported that Ni incorporation improves electrical conductivity and structural stability by facilitating LDH phase retention under alkaline conditions. Moreover, the coexistence of LDH and spinel phases has been shown to significantly improve electron mobility and exposure of catalytically active sites. Despite these advances, there is a lack of systematic studies that correlate metal composition, post-synthesis treatment, and the phase structure with OER/HER performance.[10,11] In particular, the effects of alkaline activation using sodium hydroxide (NaOH) or potassium hydroxide (KOH)/urea – a post-treatment known to increase surface hydroxylation, porosity, and defect density – remain underexplored in trimetallic oxide systems [12,13]

In this study, we address these research gaps by synthesizing CoFeNiOx electrocatalysts via a simple hydrothermal method, followed by thermal annealing and alkaline post-treatment. By tuning the CoFeNi molar ratio (1:1:1, 1:3:1, and 3:1:1), we systematically investigate the relationship between composition, phase evolution, and electrochemical performance.[12,13] Based on morphological analysis, Co-rich samples have a rougher, more porous surface, particularly after KOH/urea activation. Structural characterization confirmed the formation of LDH and spinel phases, including nickel(II) iron(III) oxide ($NiFe_2O_4$) and cobalt(II,III) oxide (Co_3O_4),[14,15] which contribute to improved electron transport and reactivity. Electrochemical measurements revealed that the CoFeNiOx (1:1:1) electrocatalyst exhibits the most favorable OER activity, with an overpotential of 270 mV at 10 mA cm^{-2}, a low Tafel slope of ~45 mV dec^{-1}, and excellent stability over 1000 cycles. Meanwhile, the CoFeNiOx (3:1:1) electrocatalyst shows better HER activity, highlighting the bifunctional potential of these catalysts.[1,16] Overall, our findings confirm that compositional control and alkaline activation are powerful tools to optimize the electrocatalytic performance of CoFeNiOx materials.[17,18] The observed synergy between redox-active Co^{3+}/Fe^{3+} sites and the structural stabilization offered by Ni^{2+} provides important insights for the rational design of next-generation water-splitting catalysts. Mechanistically, we show that synergy in CoFeNiOx electrocatalysts arises from

Fe-induced electron redistribution that stabilizes higher-valent Co/Ni oxyhydroxides, LDH–spinel heterointerfaces that lower charge-transfer resistance, and a higher fraction of surface M–OH sites that correlates with OER activity.

2. EXPERIMENTAL SECTION

2.1. *Materials and reagents*

Cobalt nitrate hexahydrate, $(CoNO_3)_2{\cdot}6H_2O$ (99.5 %); iron(III) nitrate nonahydrate, $Fe(NO_3)_3{\cdot}9H_2O$ (≥ 99 %); nickel nitrate hexahydrate, $Ni(NO_3)_2{\cdot}6H_2O$ (99.5 %); ethanol, CH_3CH_2OH (99.7%); KOH, and *N*,*N*-dimethyl formamide (DMF, 99.5 %) were purchased from Sino Pharm Chemical Reagent Co, Ltd. (China). Carbon cloth (CC) was purchased from DuPont China Holding Co., Ltd. (China). Hydrochloric acid (HCl) and 2,5-dihydroxyterephthalic acid ($C_8H_6O_6$, 98%) was obtained from China. Ammonium chloride (NH_4Cl) and urea (NH_2CONH_2) were also obtained from Sino Pharm Chemical Reagent Co, Ltd. (China). Carbon cloth (CC) was purchased from DuPont China Holding Co., (China). 4,4′-Biphenyldicarboxylic acid (H_2bpdc, $C_{14}H_{10}O_4$, ≥ 98%) was obtained from Beijing HWRK Chem Co., LTD (China). All chemical reagents were of analytical grade and used without any further purification. Experiments used only deionized water.

2.2. *Synthesis of CoFeNi metal–organic framework (MOFs)*

For synthesis, 0.50 mmol of H_2bpdc was dissolved in 30 ml of DMF (0.017 M**)** with sonication until complete dissolution (pH ~6.8). The solution was placed in a 50 ml Teflon liner containing pre-cleaned CC and heated at 120 °C for 6 h.

2.3. *Synthesis of CoFeNi LDH from CoFeNi MOFs*

Solution A was prepared by mixing $Co(NO_3)_2{\cdot}6H_2O$, $Fe(NO_3)_3{\cdot}9H_2O$, and $Ni(NO_3)_2{\cdot}6H_2O$. Five formulations were prepared, with Fe:Co:Ni molar ratios of 0:1:1, 1:9:1, 1:3:1, 1:1:1, and 3:1:1 (the amount of metal ions was maintained at 5.00 mmol). To each formulation, 4.33 mmol of urea and 2.16 mmol NH_4F were added in 30 ml of deionized water. The initial pH of the solution was 6.1. Nickel foam (NF; 1.5 × 1.5 cm^2) was soaked in 1 M HCl for 20 min and washed with deionized water and absolute ethanol. Then, solution A was transferred to a 50 ml Teflon liner in which the NF was supported by a Teflon stand; the mixture was heated at 180 °C for 6 h in a stainless-steel autoclave. The precipitate deposited on the NF was rinsed three times with deionized water and absolute ethanol, and then dried in an oven at 60 °C for 12 h.

2.4. *Synthesis of oxides from LDHs*

The dried CoFeNi LDH precursor was calcined at 400 °C for 4 h under flowing Ar (100 standard cm^3 min^{-1}) in a tubular furnace. The heating ramp rate was 6 °C min^{-1}. The sample was cooled naturally to room temperature under continuous argon flow.

$$\text{CoFeNi LDH} \xrightarrow{\text{heat}} \text{CoFeNiOx}$$

2.5. *Material characterization*

X-ray powder diffraction (XRD) was performed with a D8 Advance (Brucker AXS, Germany) with Cu-K radiation at a scanning rate of 2° min^{-1} in the 2θ range of 5°–90°. X-ray photoelectron spectroscopy (XPS) was carried out on an ESCLAB 250Xi spectrophotometer (Thermo Fisher Scientific, USA) to analyze the valence state. XPS spectra were referenced to the C 1s peak of 284.8 eV. The morphology was characterized by field emission scanning electron microscopy (FESEM, Gemini SEM 300, Carl Zeiss, Germany). Transmission electron microscopy (TEM) was performed with a JEM 2100 (JEOL Ltd., Japan) to examine lattice fringe.

2.6. *Electrochemical measurements*

A CHI 760 electrochemical workstation (CHI Instruments, Shanghai Chenhua Instrument Corp., China) in a standard three-electrode system at room temperature was used for electrochemical testing. The as-prepared electrocatalysts, mercury/mercury oxide (Hg/HgO) electrode, and graphite rod were used as the working, reference, and counter electrodes, respectively. The catalyst loading on CC was calculated from the mass difference before and after deposition; it was approximately 1.5 mg cm^{-2}. For all measurements, the potentials were calculated with respect to reversible hydrogen electrode (RHE) based on the following equation:

$$E(\text{RHE}) = E(\text{SCE}) + 0.059 \times \text{pH} + 0.242\ \text{V}$$

Linear sweep voltammetry (LSV) curves were generated in 1 M KOH (as an electrolyte)

with a scan rate of 2 mV s^{-1}; they were generated after 20 cycles of cyclic voltammetry (CV) to stabilize the current. All polarization potentials were calibrated with 85 % iR compensation. CV curves with different scan rates (10–100 mV s^{-1}) were determined over a potential range in which redox processes were absent to calculate the electrochemical double-layer capacitance:

$$cdl = \frac{(ja - jc)}{2v} = \frac{ja + |jc|}{2v} = \frac{\Delta j}{2v}$$

where *Cdl* is the double-layer capacitance of the electroactive materials; *ja* and *jc* are the anodic and cathodic current density (mA cm^{-1}), respectively, recorded at the middle of the selected potential range; and *v* is the scan rate (mV s^{-1}). Electrochemical impedance spectroscopy (EIS) was operated on the same standard three-electrode glass cell system in 1 M KOH (as an electrolyte) with a frequency range of 0.01–100 kHz and an amplitude of 5 mV. Cycling stability was tested by observing the LSV polarization curve before and after 1,000 continuous CV cycles at a scan rate of 100 mV s^{-1}. Long-term stability was evaluated using chronopotentiometry at a constant current density of 10 mA cm^{-1}. Unless otherwise stated in the figure captions, measurements were at room temperature (~25 °C) with 85 % iR compensation, and a $CoFeNiO_x$/CC geometric area of 1.0 cm^2.

3. RESULTS AND DISCUSSION

Scheme 1 illustrates the stepwise synthesis and structural evolution of the $CoFeNiO_x$ electrocatalyst. The process begins with the fabrication of a CoFeNi MOF via a solvothermal method, yielding a highly ordered precursor supported on a conductive substrate.[19] In the second step, this MOF is transformed into a CoFeNi LDH structure through hydrothermal conversion, allowing for the generation of a mixed metal hydroxide phase with enhanced surface area and active site accessibility.[20] The final thermal annealing step under an inert atmosphere facilitates the conversion of the LDH into a nanocrystalline CoFeNiOx mixed metal oxide, achieving a robust, catalytically active surface with favorable morphology and electronic properties for water-splitting applications.

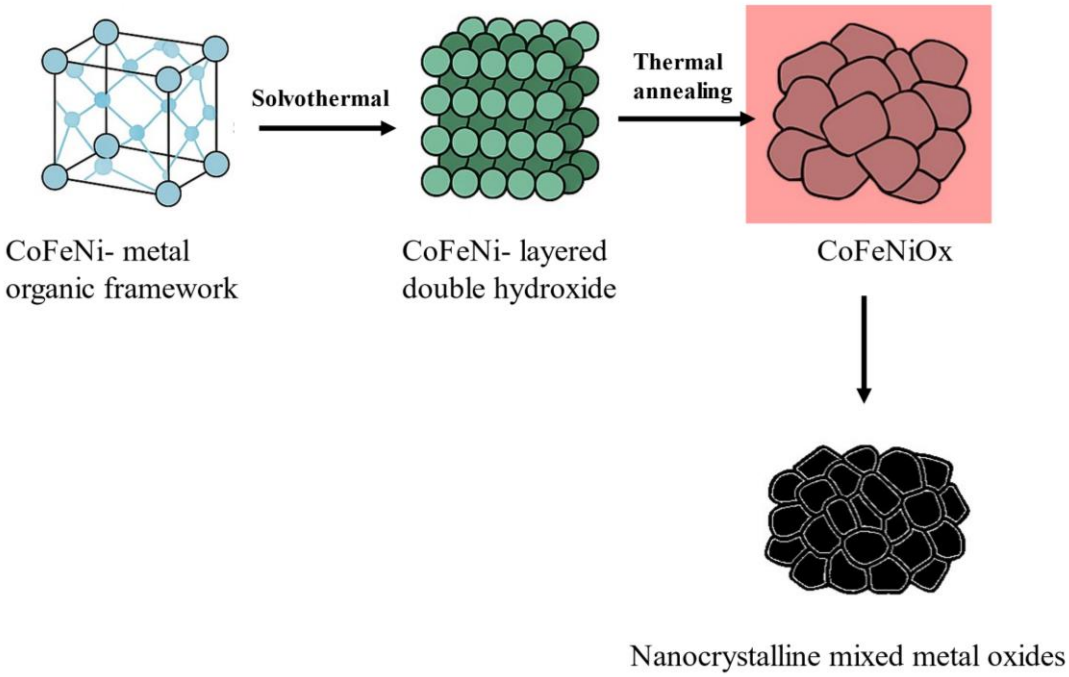

Scheme 1. The stepwise synthesis of CoFeNiOx mixed metal oxides on CC for water splitting

3.1. *Phase composition and crystallinity*

The XRD patterns of the synthesized $CoFeNiO_x$ (1:1:1) and (3:1:1) electrocatalysts show clear crystalline characteristics, indicating the formation of mixed metal oxide phases (Fig. 1). The peaks correspond to the spinel-type structures usually formed for Co_3O_4, $NiFeO_4$, and other Co-Fe-Ni oxides. For both molar ratios, peak broadening corresponds to the nano-scale of crystals and large sur-

face area, properties that are advantageous for electrocatalysis.[21] Remarkably, the CoFeNiO$_x$ (3:1:1) electrocatalyst shows a slightly sharper peak, which suggest greater crystallinity, presumably because the highly Co-enriched environment favors a well-defined lattice structure. The changes in the metal precursors to their oxides are denoted by the loss of nitrate associated signals as well as metal-oxygen coordination reflections. These trends also confirm that treatment using NaOH and KOH/urea successfully triggered hydrolysis and carbonate formation to promote crystal growth and stabilization.

The XRD patterns of the CoFeNiO$_x$ electrocatalysts reveal characteristic peaks at approximately 11.2° and 31.3°, indicating the presence of an LDH structure (planes 003 and 012). Additionally, peaks at ~36.8° and 44.8° correspond to the (311) and (400) planes of Co_3O_4, suggesting partial spinel phase formation.[22] A peak at ~59.3° is attributed to the (511) plane of $NiFe_2O_4$. These results confirm the coexistence of LDH and spinel oxide phases in the synthesized electrocatalysts, highlighting the influence of metal composition on the crystalline structure.

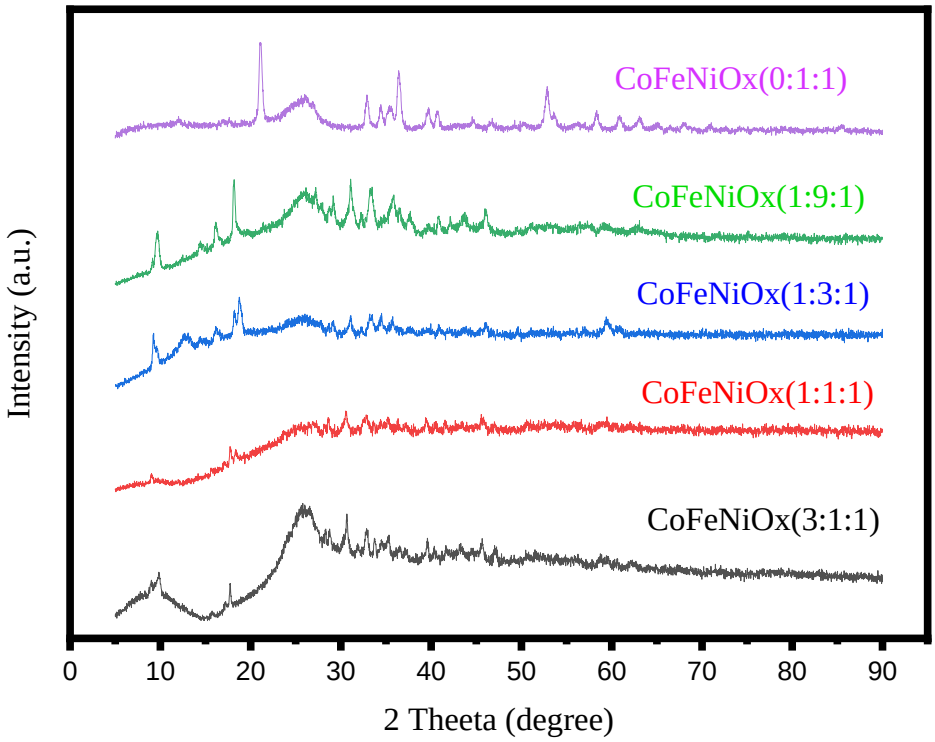

Fig. 1. XRD patterns of the CoFeNiOx electrocatalysts with different molar ratios

3.2. *Characterization*

SEM was used to examine the surface morphology and textural features of the synthesized electrocatalysts anchored on CC (Figure 2). The CoFeNiOx (1:1:1) electrocatalyst exhibits a distinctive flower-like or rosette morphology composed of thin, porous nanosheets that are interconnected (Figure 2a–c). The flower-like, layered morphology of the CoFeNiOx (1:1:1) electrocatalyst provides a high surface area and abundant active sites, facilitating efficient ion and electron transport. The CoFeNiOx (1:3:3) electrocatalyst consists of granular, irregular nanoparticles and clustered platelets with small rod- or needle-like structures growing in bundles and less pronounced roughness (Figure 2d–f). The CoFeNiOx (3:1:1) electrocatalyst shows a mixed structure with both sheet-like and particle-like elements with denser clusters and stacked nanosheets (Figure 2g–i). The consistent formation of hierarchical nanosheet arrays indicates that the composition strongly influences porosity and surface roughness. This optimized structure enhances electrocatalytic performance by improving reactant accessibility and promoting faster charge transfer.[24] Conversely, the more aggregated, granular structure of the CoFeNiOx (1:3:3) electrocatalyst and the needle-like hierarchical network of the CoFeNiOx (3:1:1) electrocatalyst result in variable surface areas and active site exposure, which affect their catalytic efficiency relative to the CoFeNiOx (1:1:1) electrocatalyst.

The micrographs demonstrate obvious surface roughness variations between the CoFeNiOx (1:1:1) and $CoFeNiO_x$ (3:1:1) electrocatalysts. The CoFeNiOx (1:1:1) electrocatalyst shows a reasonably smooth surface, moderate porosity, and particle clusters.[23] Conversely, the CoFeNiOx (3:1:1) electrocatalyst has a rougher surface with granular characteristics and distinct voids. These features are likely due to increased nucleation kinetics from Co enrichment. The porous structure for the CoFeNiOx (3:1:1) electrocatalyst could enhance electrolyte movement and gas diffusion, features that are critical for the OER and HER. Furthermore, the KOH/urea-treated samples have more defects and thus would provide additional active catalytic sites for redox reactions.

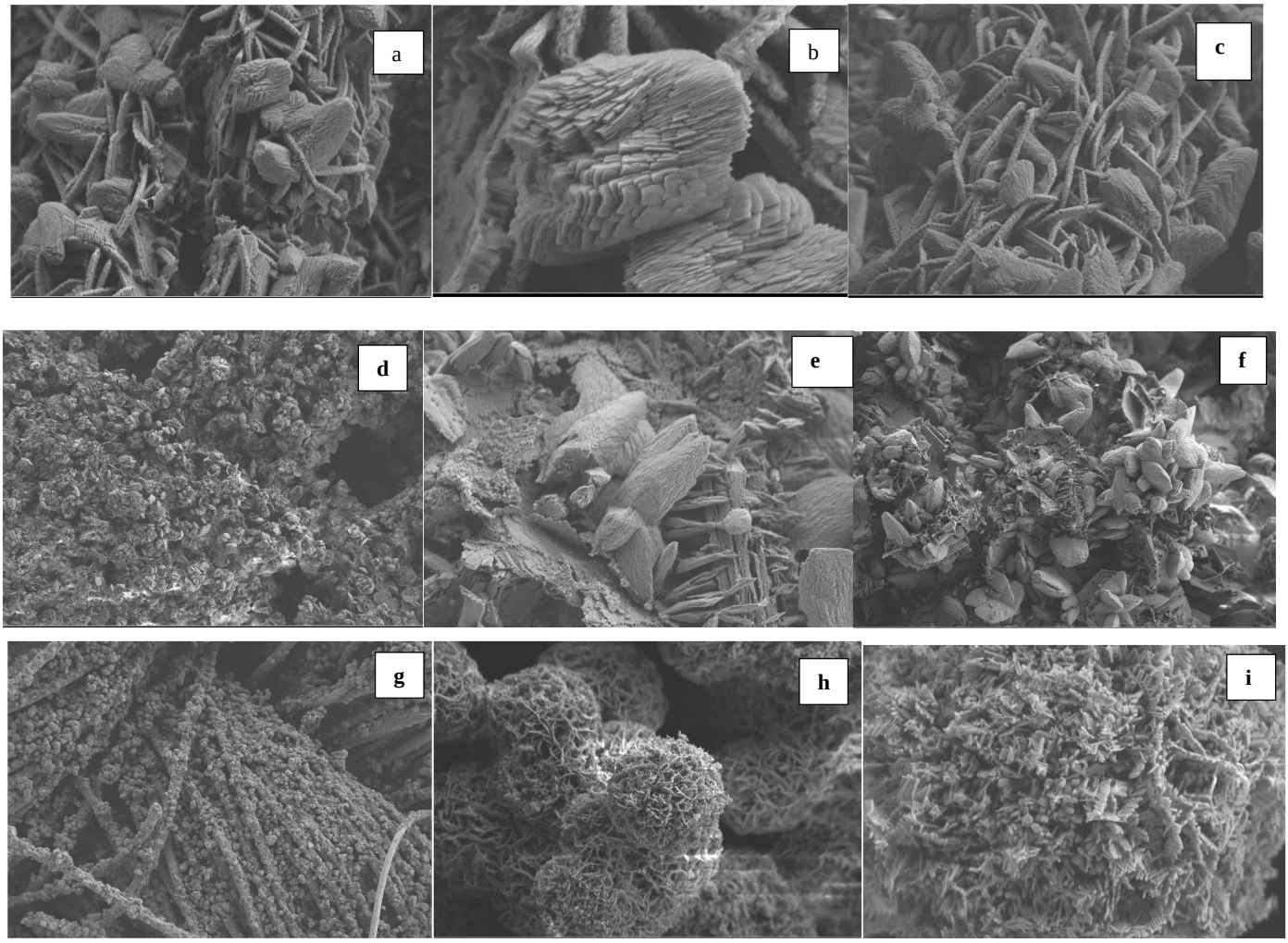

Fig. 2. FESEM images of the (a–c) CoFeNiOx (1:1:1), (d–f) CoFeNiOx (1:3:3), and (g–i) CoFeNiOx (3:1:1) electrocatalysts. Each set of images shows low-, medium-, and high-magnification views to highlight the overall morphology, nanosheet texture, and porous structure. Scale bars: 1 μm (a, d, and g), 500 nm (b, e, and h), and 200 nm (c, f, and i)

We used TEM to examine the structural and chemical composition of the CoFeNiOx electrocatalysts. As shown in Figure 3a–c, the CoFeNiOx (1:1:1) electrocatalyst consists of ultrathin nanosheets, with the high-resolution TEM image (Figure 3b) revealing lattice fringes with an interplanar spacing of 0.21 nm, corresponding to the (400) plane of spinel $CoFe_2O_4$. The CoFeNiOx (1:3:1) electrocatalyst (Figure 3a-c–displays partially aggregated nanoparticles embedded within sheet-like structures, whereas the CoFeNiOx (3:1:1) electrocatalyst (Figure 3a-c–exhibits well-defined crystalline fringes indicative of Co_3O_4-rich domains. The as-synthesized CoFeNiOx (1:1:1) electrocatalyst contains nanoparticles that are approximately 50 nm in diameter, surrounded by smaller 10–20 nm particles uniformly distributed around each primary particle (Figure 3b–c).[25] This hierarchical structure promotes efficient charge transfer and exposes abundant active sites, enhancing OER kinetics and reducing the required overpotential.

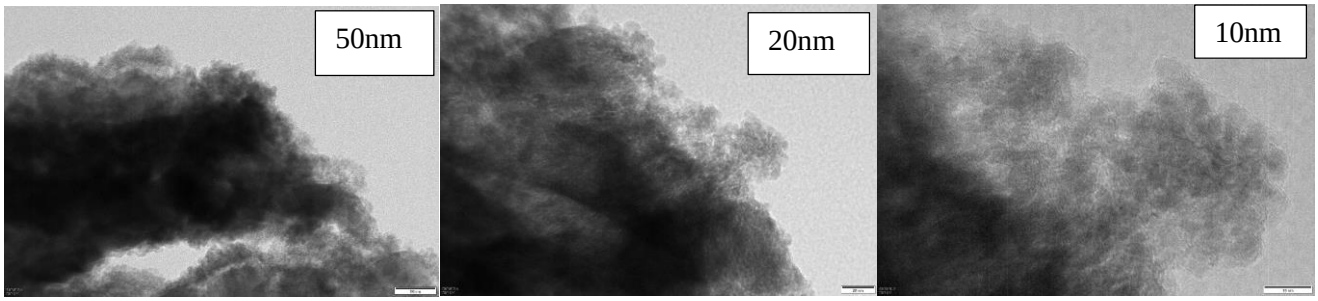

Fig. 3. TEM images of the CoFeNiOx (1:1:1) electrocatalyst. (a) A low-magnification image showing nanosheet clusters (the scale bar is 50 nm). (b) A high-resolution image highlighting lattice fringes with d-spacing of 0.21 nm indexed to the (400) plane of Co_3O_4 (the scale bar is 20 nm). (c) A high-resolution image showing uniformly distributed nanoparticles of 10–20 nm surrounding the nanosheets (the scale bar is 10 nm)

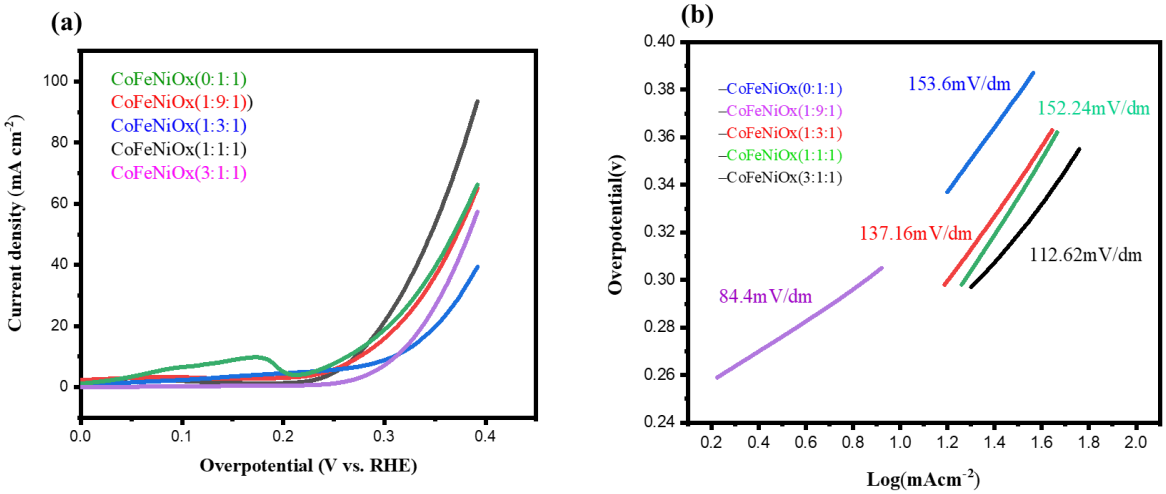

Fig. 4. (a) LSV curves and (b) corresponding Tafel slopes of the CoFeNiO$_x$ electrocatalysts with different molar ratios (0:1:1, 1:9:1, 1:3:1, 1:1:1, and 3:1:1) measured in 1 M KOH (as an electrolyte) using a three-electrode system (CoFeNiOx/CC as the working electrode, Hg/HgO as the reference electrode, and a graphite counter). LSV curves were recorded at a scan rate of 2 mV s^{-1} with 85% iR compensation applied

Figure 4a depicts the LSV curves for the commercial CoFeNiO$_x$ electrocatalysts during the OER. At a current density of 10 mA cm^{-2}, the resulting CoFeNiO$_x$ (1:1:1) electrocatalyst requires only 264 mV of overpotential, surpassing the overpotential of 272 mV for the CoFeNiO$_x$ (0:1:1) electrocatalyst, 276 mV for the CoFeNiO$_x$ (1:9:1) electrocatalyst, 309 mV for the CoFeNiO$_x$ (1:3:1) electrocatalyst, and 312 mV for the CoFeNiO$_x$ (1:3:3) electrocatalyst. The formation of oxides and spinel phases like Co_3O_4 and $NiFe_2O_4$[27] stands out as a pivotal factor in augmenting the electrocatalytic activity.

The LSV curves and corresponding Tafel slopes clearly demonstrate that the CoFeNiO$_x$ (1:1:1) electrocatalyst exhibits superior OER performance in 1 M KOH (Figure 4), achieving the highest current densities at the lowest overpotentials.[26] To contextualize the activity of the CoFeNiO$_x$ (1:1:1) electrocatalyst, we compared its overpotential at 10 mA cm^{-2} (η_{10}), Tafel slope, and stability with noble-metal oxides (RuO_2 and IrO_2) and a leading earth-abundant reference (NiFe-LDH) under alkaline conditions (1.0 M KOH). Based on the literature, RuO_2 achieves $\eta_{10} \approx 240$–300 mV with Tafel slopes ~50–80 mV dec^{-1} (e.g., nanoporous RuO_2: η_{10} = 240 mV, Tafel = 75 mV dec^{-1}), and IrO_2 shows $\eta_{10} \approx 260$–320 mV with Tafel ~45–70 mV dec^{-1} (e.g., IrO_2-based systems: $\eta_{10} \approx 266$ mV, Tafel ≈ 56 mV dec^{-1}). Advanced NiFe-LDH catalysts typically show $\eta_{10} \approx 205$–243 mV and Tafel ~60–80 mV dec^{-1} in 1.0 M KOH. In comparison, our CoFeNiO$_x$ (1:1:1) electrocatalyst on CC delivers η_{10} = 264 mV and Tafel = 84.4 mV dec^{-1}, which is competitive with IrO_2/RuO_2 and within the reported range of high-performing NiFe-LDH materials when accounting for differences in substrate, loading, and iR-correction protocols. We

followed recent benchmarking guidance to ensure like-for-like comparison and report stability at 10 mA cm^{-2} over 24 h alongside activity metrics. This is further confirmed by its low Tafel slope of 84.4 mV dec^{-1}, indicating favorable reaction kinetics and charge transport characteristics. In contrast, the $CoFeNiO_x$ (1:9:1) and $CoFeNiO_x$ (0:1:1) electrocatalysts require higher overpotentials and present larger Tafel slopes (~152–154 mV dec^{-1}), suggesting slower reaction dynamics. Overall, the results highlight the pivotal role of the optimized CoFeNi ratio in enhancing both the activity and kinetics of the OER in alkaline conditions.

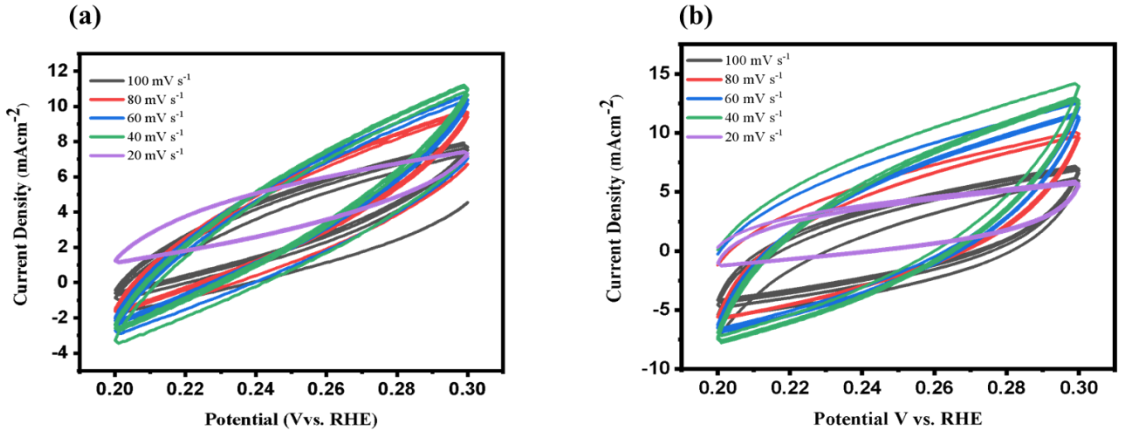

Fig. 5. CV curves of the (a) $CoFeNiO_x$ (1:1:1) and (b) $CoFeNiO_x$ (3:1:1) electrocatalysts, recorded in 1 M KOH (as an electrolyte) within the non-Faradaic potential window (0.15–0.45 V vs. the RHE) at various scan rates (10–100 mV s^{-1}). Data were collected to estimate Cdl as a measure of ECSA

Figure 5 shows the CV curves of the CoFeNiOx (1:1:1) and (3:1:1) electrocatalysts measured at different scan rates. The CoFeNiOx (1:1:1) electrocatalyst exhibits the largest Cdl, indicating the greatest electrochemically active surface area (ECSA) and consistent with the fact that it had the lowest OER overpotential (264 mV at 10 mA cm^{-2}) and favorable Tafel slope (84.4 mV dec^{-1}). In contrast, the CoFeNiOx (0:1:1) and (1:9:1) electrocatalysts display significantly smaller Cdl values, correlating with their poorer OER activity. The CoFeNiOx (3:1:1) electrocatalyst shows a moderate Cdl value and demonstrates enhanced HER activity, suggesting that its surface sites are more suited for proton reduction than the OER. These results confirm that the rougher surface and increased defect density for the $CoFeNiO_x$ (1:1:1) electrocatalyst, combined with urea/KOH activation, effectively increase active site exposure and facilitate charge transfer, thereby accounting for its superior electrocatalytic behavior.

The ECSA of the electrocatalysts was determined based on CV measurements in 1 M NaOH across a range of potential scan rates (from approximately 20 to 100 mV s^{-1}), with potential variations spanning from 0.15 to 0.45 V versus the RHE (Fig. 6).[28] The CV curves exhibit a pseudo-rectangular shape, devoid of discernible Faradic processes. A higher value implies the presence of a larger number of exposed active sites, which facilitates and promotes various electrochemical processes.[29] Increased accessibility to active sites enhances the efficiency and effectiveness of electrochemical reactions.[30] There is a linear relationship for all electrocatalysts, confirming the reliability of the measurements. Notably, the $CoFeNiO_x$ (1:1:1) electrocatalyst has the steepest slope, corresponding to the fact that it has the largest Cdl value, which indicates a greater number of electrochemically accessible active sites. This finding is consistent with its superior OER performance, as evidenced by the lowest overpotential (264 mV at 10 mA cm^{-2}) and the most favorable Tafel slope (84.4 mV dec^{-1}). In contrast, the CoFeNiOx (0:1:1) and (1:9:1) electrocatalysts show much smaller slopes, reflecting limited surface site exposure and slower reaction kinetics, while the CoFeNiOx (3:1:1) electrocatalyst presents an intermediate Cdl value that aligns with its moderate OER and relatively stronger HER activity. Taken together, these results highlight that optimization of the CoFeNiOx composition coupled with alkaline/urea activation enhances the accessible surface area, thereby accelerating charge transfer and improving catalytic performance.

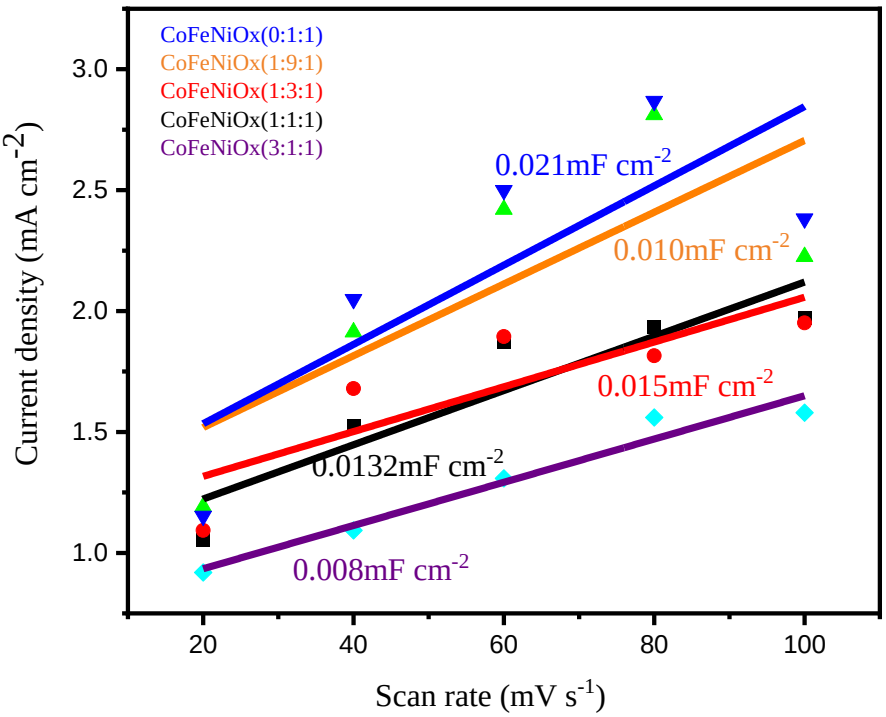

Fig. 6. Plots of Δj = (ja − jc) versus the scan rate for the CoFeNiO$_x$ electrocatalysts obtained from the CV curves measured in the non-Faradaic potential window (0.15–0.45 V vs. the RHE) in 1 M KOH (as an electrolyte). The CV curves were recorded at a scan rate of 10–100 mV s^{-1}, and Δj was determined at the midpoint potential

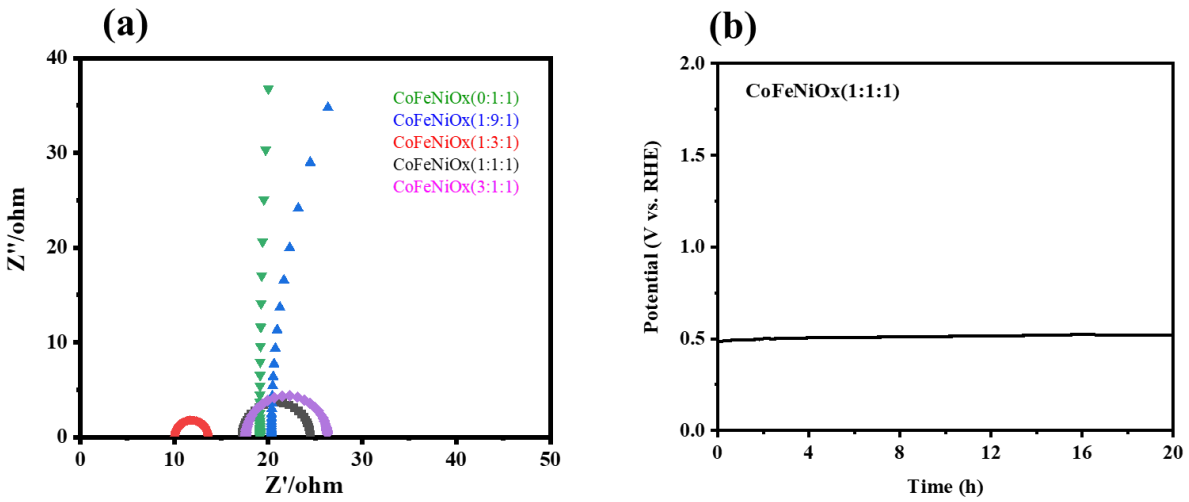

Fig. 7. (a) EIS Nyquist plots of the CoFeNiOx electrocatalysts measured in 1 M KOH (as an electrolyte) at 0.43 V versus the RHE under OER conditions, over the frequency range of 0.01 Hz to 100 kHz with an AC amplitude of 5 mV. (b) Chronopotentiometry stability test of the CoFeNiOx (1:1:1) electrocatalyst on CC at a constant current density of 10 mA cm^{-2} in 1 M KOH, recorded for 24 h with 85 % iR compensation

Figure 7a presents the Nyquist plots of the electrocatalysts during the OER at 0.43 V. Notably, the CoFeNiO$_x$ (1:1:1) electrocatalyst stands out due to its remarkably low charge-transfer resistance (Rct) compared with the other catalysts. This observation suggests an exceptionally rapid exchange of charges and surface reactions at the interface between the electrode and the electrolyte. The reduced Rct value underscores the efficient electron transfer processes and increased[31] catalytic activity of the CoFeNiO$_x$ (1:1:1) electrocatalyst, indicating its potential electrochemical applications to enhance performance. Figure 7b presents the chronopotentiometry curve of the CoFeNiO$_x$ (1:1:1) electrocatalyst at a current density of 10 mA cm^{-2}. Impressively, even after continuous catalysis for 24 h, there is only a marginal 40 mV increase in overpotential.[32] These results under-

score the exceptional durability and cycle stability of the $CoFeNiO_x$ (1:1:1) electrocatalyst for the OER.

FESEM revealed that the CoFeNiOx (1:1:1) electrocatalyst undergoes both morphological and compositional changes during the OER (Figure 8). After 1000 CV cycles within a potential window of 0.45–0.55 V versus the RHE, the electrocatalyst transforms from a flower-like structure to sheet-like nanosheets. XRD analysis (Figure 1) indicates the formation of mixed metal oxides and hydroxides, species known to enhance OER activity. The survey XPS spectrum (Figure 9e) confirms the presence of Co, Fe, Ni, C, and O, indicating that the elemental composition is largely preserved after long-term cycling.

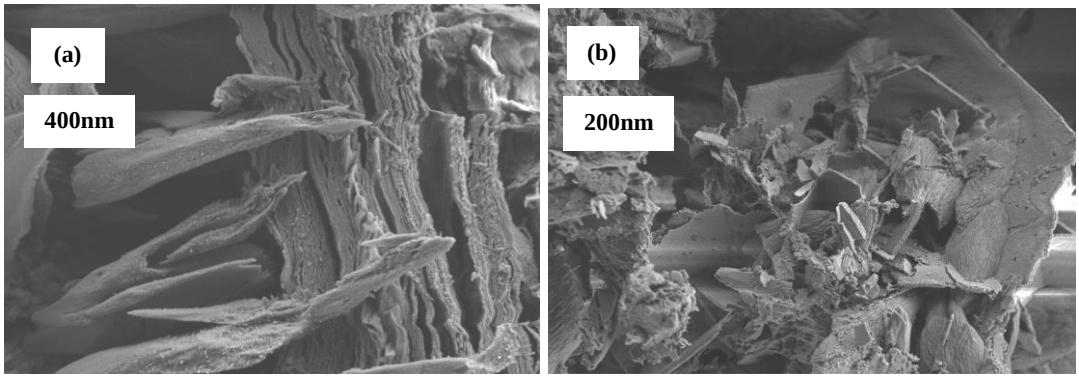

Fig. 8. FESEM images of $CoFeNiO_x$ (1:1:1) after 1000 cv cycles

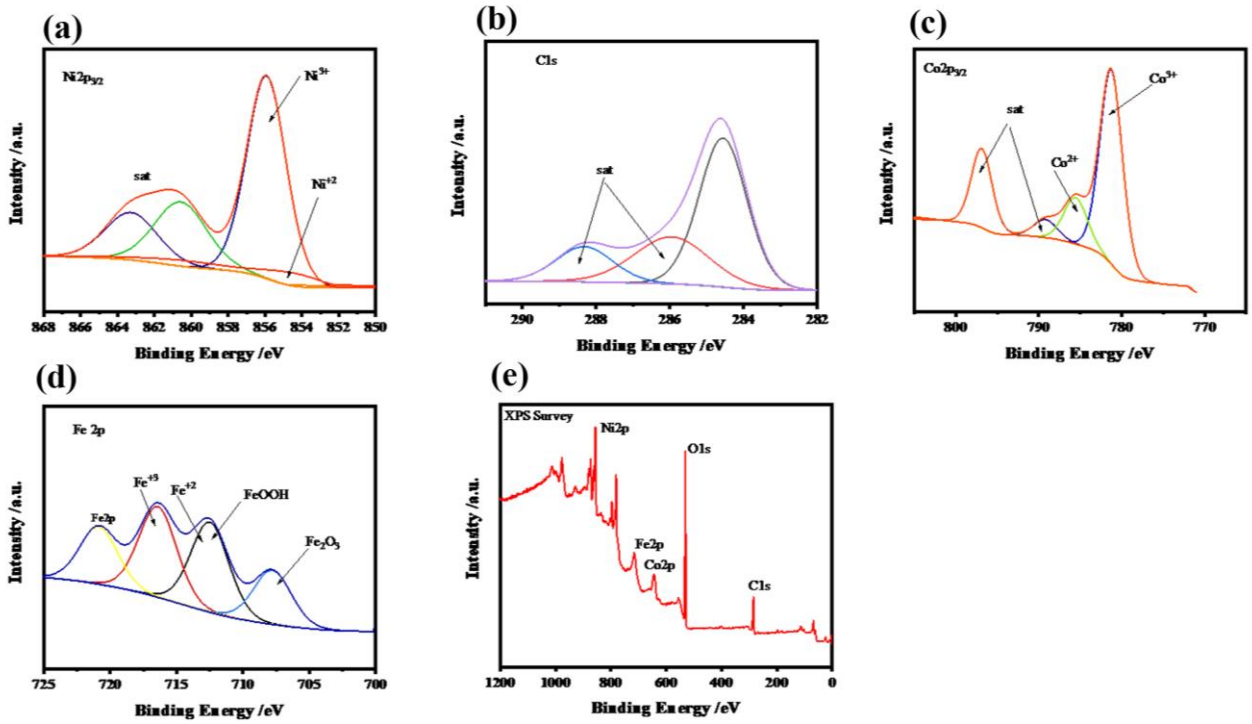

Fig. 9. High-resolution XPS (a) Ni 2p, (b) C 1s, (c) Co 2p, and (d) Fe 2p spectra for the CoFeNiOx (1:1:1) electrocatalyst. (e) The XPS survey spectrum for the CoFeNiOx (1:1:1) electrocatalyst

3.3. *The mechanism underlying Co-Fe-Ni synergy*

The incorporation of Fe into Co/Ni oxides induces electronic synergy, tuning Co and Ni toward higher-valent, OER-active states. High-resolution XPS reveals surface enrichment of trivalent species across all cations: Ni^{3+} at 58.5% ± 2.0% (compared with Ni^{2+} at 41.5% ± 2.0%), Co^{3+} at 60.8% ± 1.8% (compared with Co^{2+} at 39.2% ± 1.8%), and Fe^{3+} at 62.3% ± 2.2% (compared with Fe^{2+} at 37.7% ± 2.2%). There is a pronounced Co $2p_{1/2}$ binding energy decrease of ≈4.25 eV (from the CoFeNi-LDH precursor to the CoFeNiOx elec-

trocatalyst), providing evidence of electron redistribution onto Co centers upon Fe incorporation, which stabilizes •OOH intermediates and lowers the OER overpotential. These electronic effects correlate with improved catalytic kinetics, as reflected in the lowest overpotential at 10 mA cm^{-2} (η_{10} = 264 mV) and a favorable Tafel slope (84.4 mV dec^{-1}) for the CoFeNiOx (1:1:1) electrocatalyst.

Interfacial synergy arises from LDH/spinel heterostructures that facilitate charge transfer. XRD and TEM confirm coexisting LDH-derived motifs with spinel domains, while SEM/TEM reveals increased surface roughness and porosity after alkaline activation. These heterointerfaces promote electron mobility and mass transport, consistent with the observed reduction in charge-transfer resistance (Rct) from the EIS measurements.

Surface-chemistry synergy further contributes to OER performance. O 1s deconvolution identifies lattice O^{2-} (529.1–529.5 eV), M–OH/OH^{2-} (530.8–531.2 eV), and adsorbates/carbonates (532.2–533.4 eV). The CoFeNiOx (1:1:1) electrocatalyst exhibits a higher M–OH fraction than the other compositions (e.g., CoFeNiOx (3:1:1)), consistent with oxyhydroxide formation under alkaline activation and during OER. Increased $M^{3+}/(M^{2+} + M^{3+})$ ratios and a higher M–OH content correlates with a larger Cdl and a lower Rct, indicating surfaces enriched in oxyhydroxide terminations that facilitate OH → O → *OOH conversion. The activity trends across the electrocatalysts display a volcano-like dependence on stoichiometry, with the CoFeNiOx (1:1:1) electrocatalyst achieving the lowest η_{10} (264 mV) compared with 272, 276, 309, and 312 mV for the CoFeNiOx (0:1:1), (1:9:1), (1:3:1), and (1:3:3) electrocatalysts. This improvement relative to the mean of the other compositions (≈28 mV) indicates a true cooperative effect beyond simple linear mixing.

We re-fitted all high-resolution XPS spectra (Ni 2p, Co 2p, Fe 2p, O 1s, C 1s) using a consistent protocol: charge correction to C 1s (sp^2/sp^3) at 284.8 eV, Shirley backgrounds, GL(m) peak shapes with 30%–40% Lorentzian contribution, and a full width at half maximum (FWHM) constrained to 1.2–1.8 eV for metals and 1.0–1.6 eV for O 1s/C 1s. We quantified the elements from the survey scans used the manufacturer's sensitivity factors. Uncertainties are reported as ±1 standard deviation from spot-to-spot variation; binding energy uncertainties are ±0.05–0.10 eV (instrumental) and ±0.10–0.20 eV including fitting. The spin-orbit splitting and area ratios are fixed (Ni 2p Δ = 17.2–17.8 eV, $2p_3/_2$:$2p_1/_2$ ≈ 2:1; Co 2p Δ = 15.0–15.6 eV; Fe 2p Δ = 13.0–13.6 eV), and we included satellite peaks for Ni^{2+}/Co^{2+} with ±0.5 eV constraints. The survey scan atomic percentages (the mean of three spots with a diameter of ~400–600 μm) are 14.3% ± 0.6% for Ni, 13.6% ± 0.5% for Co, 12.9% ± 0.5% for Fe, 48.2% ± 1.5% for O, and 11.0% ± 1.0% for C (Figure 9e), consistent with the designed stoichiometry. The Fe 2p spectra (Figure 9d) show Fe $2p_3/_2$ and $2p_1/_2$ peaks at 711.2 and 723.4 eV, with satellites at 709.1 and 724.1 eV, confirming the presence of Fe^{2+} alongside Fe^{3+} (62.3%). The Ni $2p_3/_2$ spectra (Figure 9a) exhibits peaks at 855.6 eV (Ni^{3+}) and 853.1 eV (Ni^{2+}), along with an associated satellite peak at ~861.5 eV,[33] and the Co 2p spectra (Figure 9c) shows peaks at 780.2 eV (Co^{3+}) and 796.0 eV (Co^{2+}), highlighting surface oxidation with trivalent cation predominance. The Co $2p_1/_2$ shift from 786.46 eV (LDH) to 781.11 eV (CoFeNiOx) reflects increased electron density at Co centers, enhancing •OOH stabilization.[2,3,4] The C 1s spectrum (Figure 9b) contains peaks at 284.8 eV (C–C/C=C), 286.2 eV (C-O/C-OH), and 288.6 eV (O=C–O), with minor satellite features, indicating surface contamination or adsorbed carbonates commonly seen in metal oxide materials exposed to air.

In summary, the XPS results validate the successful incorporation of Fe, Ni, and Co into the ternary $CoFeNiO_x$ (1:1:1) electrocatalyst with a surface enriched in trivalent species. The electron redistribution upon Fe doping, evidenced by shifts in binding energies, further enhances the catalytic potential for water oxidation. Urea/KOH activation alters the precursor into an oxyhydroxide-rich surface, as evidenced by O 1s deconvolution (enhanced M-OH component) and increased trivalent fractions in Ni/Co/Fe 2p, indicating stronger metal–oxygen covalency and more OOH-ready sites. Consequently, the activated sample shows lower charge-transfer resistance and improved OER kinetics (lower η_{10} and Tafel) relative to the inactivated precursor, confirming that chemical reconstruction rather than changes only to the surface area are responsible for the gain in performance.

4. CONCLUSION

This study establishes a clear composition–structure–performance relationship for CoFeNiOx water-splitting electrocatalysts. Hydrothermal synthesis followed by annealing and alkaline activation produces mixed LDH/spinel frameworks whose OER activity depends strongly on the cation ratios. Among the tested compositions, the CoFeNiOx (1:1:1) electrocatalyst exhibits the best

performance, achieving an overpotential of 264 mV at 10 mA cm^{-2} with a Tafel slope of 84.4 mV dec^{-1} in 1 M KOH, and maintaining stable operation over 24 h with only a modest increase in overpotential. XPS analysis confirms mixed valence states and a surface enriched in trivalent cations, consistent with the formation of active oxyhydroxide species under OER conditions. These findings indicate a synergistic effect among Co, Fe, and Ni, enhancing charge transfer and stabilizing reaction intermediates. Mechanistically, this synergy arises from Fe-assisted generation of high-valent Co/Ni species, improved interfacial charge transfer across LDH–spinel heterostructures, and oxyhydroxide-rich surfaces that facilitate •OOH formation.

The limitations of this study include the absence of direct porosity measurements and *in situ* spectroscopic characterization. Future work will incorporate Brunauer–Emmett–Teller (BET) surface area and pore distribution analyses, as well as benchmarking against additional state-of-the-art catalysts under identical testing conditions.

REFERENCES

(1) Guo, Y.; Park, T.; Yi, J. W.; Henzie, J.; Kim, J.; Wang, Z.; Jiang, B.; Bando, Y.; Sugahara, Y.; Tang, J.; Yamauchi, Y. Nanoarchitectonics for Transition-Metal-Sulfide-Based Electrocatalysts for Water Splitting. *Adv. Mater.* **2019**, *31* (17), 1–34. https://doi.org/10.1002/adma.201807134

(2) Hashmi, Y.; Wang, J.; Yu, F. Structurally Engineered Cobalt−iron Layered Double Hydroxide on Metal Organic Framework Electrocatalyst for Enhanced Electrocatalytic Water Splitting Performance. *Maced. J. Chem. Chem. Eng.* **2025**, *44* (1), 1–12. https://doi.org/10.20450/mjcce.2025.3101

(3) Turner, J. A. Sustainable Hydrogen Production. *Science (80-.).* **2004**, *305* (5686), 972–974. https://doi.org/10.1126/science.1103197

(4) Zhang, Y.; Guo, H.; Yuan, P.; Pang, K.; Cao, B.; Wu, X.; Zheng, L.; Song, R. Structural Evolution of CoMoO4 to CoOOH by Ion Electrochemical Etching for Boosting Oxygen Evolution Reaction. *J. Power Sources* **2019**, *442* (September), 227252. https://doi.org/10.1016/j.jpowsour.2019.227252

(5) Li, P.; Ruan, C.; Xu, J.; Xie, Y. Supercapacitive Performance of CoMoO4 with Oxygen Vacancy Porous Nanosheet. *Electrochim. Acta* **2020**, *330*. https://doi.org/10.1016/j.electacta.2019.135334

(6) Zhou, Y.; Wang, Z.; Pan, Z.; Liu, L.; Xi, J.; Luo, X.; Shen, Y. Exceptional Performance of Hierarchical Ni–Fe (Hydr)Oxide@NiCu Electrocatalysts for Water Splitting. *Adv. Mater.* **2019**, *31* (8), 1–8. https://doi.org/10.1002/adma.201806769

(7) Chen, Z.; Wang, X.; Han, Z.; Zhang, S.; Pollastri, S.; Fan, Q.; Qu, Z.; Sarker, D.; Scheu, C.; Huang, M.; Cölfen, H. Revealing the Formation Mechanism and Optimizing the Synthesis Conditions of Layered Double Hydroxides for the Oxygen Evolution Reaction. *Angew. Chemie - Int. Ed.* **2023**, *62* (10). https://doi.org/10.1002/anie.202215728

(8) Sun, H.; Chen, L.; Lian, Y.; Yang, W.; Lin, L.; Chen, Y.; Xu, J.; Wang, D.; Yang, X.; Rümmerli, M. H.; Guo, J.; Zhong, J.; Deng, Z.; Jiao, Y.; Peng, Y.; Qiao, S. Topotactically Transformed Polygonal Mesopores on Ternary Layered Double Hydroxides Exposing Under-Coordinated Metal Centers for Accelerated Water Dissociation. *Adv. Mater.* **2020**, *32* (52). https://doi.org/10.1002/adma.202006784

(9) Du, X.; Fu, J.; Zhang, X. NiCo2O4@NiMoO4 Supported on Nickel Foam for Electrocatalytic Water Splitting. *ChemCatChem* **2018**, *10* (23), 5533–5540. https://doi.org/10.1002/cctc.201801419

(10) Wang, Y.; Yan, D.; El Hankari, S.; Zou, Y.; Wang, S. Recent Progress on Layered Double Hydroxides and Their Derivatives for Electrocatalytic Water Splitting. *Adv. Sci.* **2018**, *5* (8). https://doi.org/10.1002/advs.201800064

(11) LIANG, X. Supporting Information Supporting Information. *Aldenderfer, Mark S., Craig, Nathan M., Speak. Robert Jeff, Popelka-Filcoff, Rachel S.* **2021**, *2* (1), 1–5.

(12) Lai, J.; Huang, B.; Chao, Y.; Chen, X.; Guo, S. Strongly Coupled Nickel–Cobalt Nitrides/Carbon Hybrid Nanocages with Pt-Like Activity for Hydrogen Evolution Catalysis. *Adv. Mater.* **2019**, *31* (2), 1–7. https://doi.org/10.1002/adma.201805541

(13) Zou, K. Y.; Li, Z. X. Controllable Syntheses of MOF-Derived Materials. *Chem. - A Eur. J.* **2018**, *24* (25), 6506–6518. https://doi.org/10.1002/chem.201705415

(14) Chen, Y. Y.; Zhang, Y.; Zhang, X.; Tang, T.; Luo, H.; Niu, S.; Dai, Z. H.; Wan, L. J.; Hu, J. S. Self-Templated Fabrication of MoNi4/MoO3-x Nanorod Arrays with Dual Active Components for Highly Efficient Hydrogen Evolution. *Adv. Mater.* **2017**, *29* (39), 1–7. https://doi.org/10.1002/adma.201703311

(15) Aghamohammadi, P.; Hüner, B.; Altıncı, O. C.; Akgul, E. T.; Teymur, B.; Simsek, U. B.; Demir, M. Recent Advances in the Electrocatalytic Applications (HER, OER, ORR, Water Splitting) of Transition Metal Borides (MBenes) Materials. *Int. J. Hydrogen Energy* **2024**, *87* (July), 179–198. https://doi.org/10.1016/j.ijhydene.2024.08.412

(16) Li, J.; Lu, S.; Huang, H.; Liu, D.; Zhuang, Z.; Zhong, C. ZIF-67 as Continuous Self-Sacrifice Template Derived NiCo2O4/Co,N-CNTs Nanocages as Efficient Bifunctional Electrocatalysts for Rechargeable Zn-Air Batteries. *ACS Sustain. Chem. Eng.* **2018**, *6* (8), 10021–10029. https://doi.org/10.1021/acssuschemeng.8b01332

(17) Tang, Y.; Fang, X.; Zhang, X.; Fernandes, G.; Yan, Y.; Yan, D.; Xiang, X.; He, J. Space-Confined Earth-Abundant Bifunctional Electrocatalyst for High-Efficiency Water Splitting. *ACS Appl. Mater. Interfaces* **2017**, *9* (42), 36762–36771. https://doi.org/10.1021/acsami.7b10338

(18) Yu, B.; Jiang, G.; Xu, W.; Cao, C.; Liu, Y.; Lei, N.; Evariste, U.; Ma, P. Construction of NiMoO4/CoMoO4 Nanorod Arrays Wrapped by Ni-Co-S Nanosheets on Carbon Cloth as High Performance Electrode for Super-

capacitor. *J. Alloys Compd.* **2019**, *799*, 415–424. https://doi.org/10.1016/j.jallcom.2019.05.353

(19) Wang, J. G.; Hua, W.; Li, M.; Liu, H.; Shao, M.; Wei, B. Structurally Engineered Hyperbranched NiCoP Arrays with Superior Electrocatalytic Activities toward Highly Efficient Overall Water Splitting. *ACS Appl. Mater. Interfaces* **2018**, *10* (48), 41237–41245. https://doi.org/10.1021/acsami.8b11576

(20) Li, Y.; Liu, J.; Chen, C.; Zhang, X.; Chen, J. Preparation of NiCoP Hollow Quasi-Polyhedra and Their Electrocatalytic Properties for Hydrogen Evolution in Alkaline Solution. *ACS Appl. Mater. Interfaces* **2017**, *9* (7), 5982–5991. https://doi.org/10.1021/acsami.6b14127

(21) Yan, Q.; Wei, T.; Wu, J.; Yang, X.; Zhu, M.; Cheng, K.; Ye, K.; Zhu, K.; Yan, J.; Cao, D.; Wang, G.; Pan, Y. Self-Supported FeNi-P Nanosheets with Thin Amorphous Layers for Efficient Electrocatalytic Water Splitting. *ACS Sustain. Chem. Eng.* **2018**, *6* (8), 9640–9648. https://doi.org/10.1021/acssuschemeng.7b04743

(22) Liu, H.; Guan, J.; Yang, S.; Yu, Y.; Shao, R.; Zhang, Z.; Dou, M.; Wang, F.; Xu, Q. Metal–Organic-Framework-Derived Co2P Nanoparticle/Multi-Doped Porous Carbon as a Trifunctional Electrocatalyst. *Adv. Mater.* **2020**, *32* (36), 1–8. https://doi.org/10.1002/adma.202003649

(23) Hao, Y.; Xu, Y.; Liu, W.; Sun, X. Co/CoP Embedded in a Hairy Nitrogen-Doped Carbon Polyhedron as an Advanced Tri-Functional Electrocatalyst. *Mater. Horizons* **2018**, *5* (1), 108–115. https://doi.org/10.1039/c7mh00706j

(24) Wang, Z.; Liu, H.; Ge, R.; Ren, X.; Ren, J.; Yang, D.; Zhang, L.; Sun, X. Phosphorus-Doped Co3O4 Nanowire Array: A Highly Efficient Bifunctional Electrocatalyst for Overall Water Splitting. *ACS Catal.* **2018**, *8* (3), 2236–2241. https://doi.org/10.1021/acscatal.7b03594

(25) Zhou, T.; Du, Y.; Wang, D.; Yin, S.; Tu, W.; Chen, Z.; Borgna, A.; Xu, R. Phosphonate-Based Metal-Organic Framework Derived Co-P-C Hybrid as an Efficient Electrocatalyst for Oxygen Evolution Reaction. *ACS Catal.* **2017**, *7* (9), 6000–6007. https://doi.org/10.1021/acscatal.7b00937

(26) Wu, Z.; Zou, Z.; Huang, J.; Gao, F. NiFe2O4 Nanoparticles/NiFe Layered Double-Hydroxide Nanosheet Heterostructure Array for Efficient Overall Water Splitting at Large Current Densities. *ACS Appl. Mater. Interfaces* **2018**, *10* (31), 26283–26292. https://doi.org/10.1021/acsami.8b07835

(27) Li, Y.; Xu, Y.; Yang, W.; Shen, W.; Xue, H.; Pang, H. MOF-Derived Metal Oxide Composites for Advanced Electrochemical Energy Storage. *Small* **2018**, *14* (25), 1–24. https://doi.org/10.1002/smll.201704435

(28) Wu, J.; Wang, D.; Wan, S.; Liu, H.; Wang, C.; Wang, X. An Efficient Cobalt Phosphide Electrocatalyst Derived from Cobalt Phosphonate Complex for All-PH Hydrogen Evolution Reaction and Overall Water Splitting in Alkaline Solution. *Small* **2020**, *16* (15), 1–9. https://doi.org/10.1002/smll.201900550

(29) Xiao, X.; Huang, D.; Fu, Y.; Wen, M.; Jiang, X.; Lv, X.; Li, M.; Gao, L.; Liu, S.; Wang, M.; Zhao, C.; Shen, Y. Engineering NiS/Ni2P Heterostructures for Efficient Electrocatalytic Water Splitting. *ACS Appl. Mater. Interfaces* **2018**, *10* (5), 4689–4696. https://doi.org/10.1021/acsami.7b16430

(30) Zhang, B.; Lui, Y. H.; Gaur, A. P. S.; Chen, B.; Tang, X.; Qi, Z.; Hu, S. Hierarchical FeNiP@Ultrathin Carbon Nanoflakes as Alkaline Oxygen Evolution and Acidic Hydrogen Evolution Catalyst for Efficient Water Electrolysis and Organic Decomposition. *ACS Appl. Mater. Interfaces* **2018**, *10* (10), 8739–8748. https://doi.org/10.1021/acsami.8b00069

(31) Narayan, N.; Meiyazhagan, A. Metal Nanoparticles as Green Catalysts. **2019**, 1–12.

(32) Kong, X. J.; Li, J. R. An Overview of Metal–Organic Frameworks for Green Chemical Engineering. *Engineering*. Elsevier Ltd August 1, 2021, pp 1115–1139. https://doi.org/10.1016/j.eng.2021.07.001

(33) Xiao, X.; Huang, D.; Fu, Y.; Wen, M.; Jiang, X. Engineering NiS / Ni 2 P Heterostructures for Efficient Electrocatalytic Water Splitting. 1–10.

(34) Zhang, G.; Li, Y.; Zhou, Y.; Yang, F. NiFe Layered-Double-Hydroxide-Derived NiO-NiFe2O4/Reduced Graphene Oxide Architectures for Enhanced Electrocatalysis of Alkaline Water Splitting. *ChemElectroChem* **2016**, *3* (11), 1927–1936. https://doi.org/10.1002/celc.201600301